

# ULRR

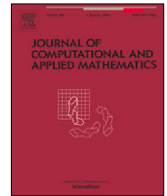
## A numerical algorithm to computationally solve the hemker problem using shishkin meshes

Item Type	Article
Authors	Hegarty, Alan F;O'Riordan, E.
Citation	Journal of Computational and Applied Mathematics;409, 11415
Publisher	Elsevier
Download date	2026-04-15 12:48:53
Item License	<a href="https://creativecommons.org/licenses/by-nc-sa/1.0/">https://creativecommons.org/licenses/by-nc-sa/1.0/</a>
Link to Item	<a href="https://hdl.handle.net/10344/11059">https://hdl.handle.net/10344/11059</a>



Contents lists available at ScienceDirect

# Journal of Computational and Applied Mathematics

journal homepage: [www.elsevier.com/locate/cam](http://www.elsevier.com/locate/cam)

## A numerical algorithm to computationally solve the Hemker problem using Shishkin meshes

A.F. Hegarty<sup>a</sup>, E. O'Riordan<sup>b,\*</sup><sup>a</sup> Department of Mathematics and Statistics, University of Limerick, Ireland<sup>b</sup> School of Mathematical Sciences, Dublin City University, Dublin 9, Ireland

### ARTICLE INFO

#### Article history:

Received 11 June 2021

Received in revised form 17 January 2022

Dedicated to the memory of P. W. Hemker, who inspired this research work

#### MSC:

65N12

65N15

65N06

#### Keywords:

Singularly perturbed

Shishkin mesh

Hemker problem

### ABSTRACT

A numerical algorithm is presented to solve a benchmark problem proposed by Hemker (1996). The algorithm incorporates asymptotic information into the design of appropriate piecewise-uniform Shishkin meshes. Moreover, different co-ordinate systems are utilized due to the different geometries and associated layer structures that are involved in this problem. Numerical results are presented to demonstrate the effectiveness of the proposed numerical algorithm.

© 2022 The Author(s). Published by Elsevier B.V. This is an open access article under the CC BY license (<http://creativecommons.org/licenses/by/4.0/>).

## 1. Introduction

In [1] Hemker proposed a model test problem in two space dimensions, defined on the unbounded domain  $\mathbb{R}^2 \setminus \{x^2 + y^2 \leq 1\}$ , which is exterior to the unit circle. The problem involves the simple constant coefficient linear singularly perturbed convection–diffusion equation

$$-\varepsilon \Delta u + u_x = 0, \quad \text{for } x^2 + y^2 > 1; \quad (1)$$

with the boundary conditions  $u(x, y) = 1$ , if  $x^2 + y^2 = 1$  and  $u(x, y) \rightarrow 0$  as  $x^2 + y^2 \rightarrow \infty$ . An exponential boundary layer and characteristic interior layers appear in the solution of this problem. In neighborhoods of the two points  $(0, \pm 1)$ , where the characteristic lines  $y = C$  of the reduced problem ( $v_x = 0$ ) are tangential to the circle, there are transition regions, where the steep gradients in the solution migrate from the exponential boundary layers (located on the left side of the unit disk) to the characteristic internal layers which are emanating from the characteristic points  $(0, \pm 1)$  (see Fig. 1). To design a numerical method, which produces stable and accurate approximations over the entire domain, for arbitrary small values of the perturbation parameter  $\varepsilon$ , is seen in [1–5] as a reasonable challenge to the numerical analysis community. Here we concentrate on the layers that appear in the vicinity of the circle by considering the problem restricted to a finite domain. Hence, we do not address the potential merging of the two characteristic layers, which can occur at a sufficiently large distance of  $O(1/\varepsilon)$  [6, pg.190] downwind (i.e.,  $x \gg 1$ ) of the circle.

\* Corresponding author.

E-mail address: [eugene.oriordan@dcu.ie](mailto:eugene.oriordan@dcu.ie) (E. O'Riordan).

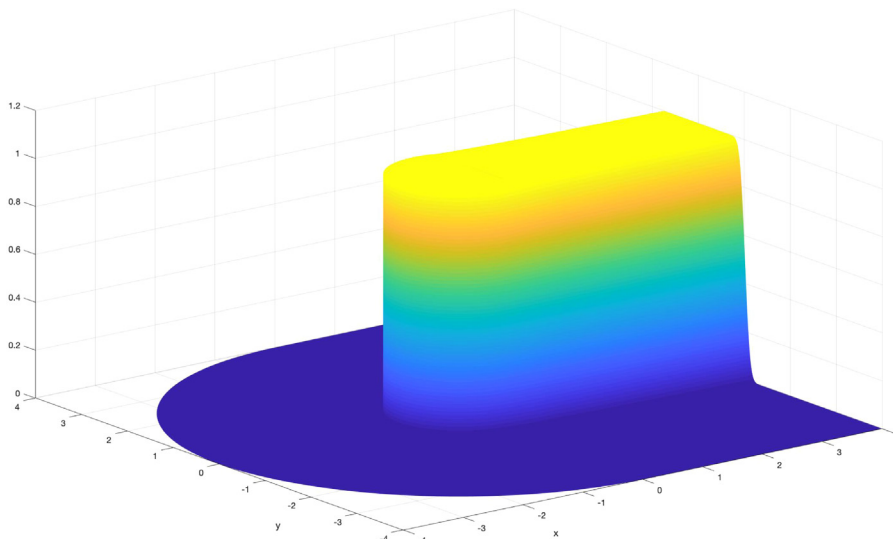


**Fig. 1.** The computed solution  $\bar{U}_2^{1024}$  of the Hemker problem (2) generated by numerical method (21) for  $\varepsilon = 2^{-10}$ .

In several publications (e.g.[2,7]) the Hemker problem is used to test the stability of numerical algorithms designed for a wide class of convection-dominated convection–diffusion problems, as classical finite element methods produce spurious oscillations for this type of singularly perturbed problems. In [8], a stable numerical method was constructed on a quasi-uniform mesh for problem (1), but there was a limited discussion of the accuracy of the numerical approximations. In this paper, we guarantee parameter-uniform stability of the discrete operators by using simple upwinded finite difference operators. Our main focus is on the design of an appropriate layer-adapted mesh, so that we guarantee that a significant proportion of the mesh points lie within the layers. In [Theorem 4](#), several pointwise bounds on the solution of the continuous problem are established, from which the location and width of any layers are identified. Asymptotic analysis [1,6,9–11] has also been used to determine the location and scale of all the layers that can appear in the solution of problem (1).

The numerical algorithm constructed in this paper is composed of several different Shishkin meshes [12] defined across different co-ordinate systems aligned to three overlapping subdomains. As we lack sufficient theoretical information about the localized character of the partial derivatives of the continuous solution, we have no meaningful pointwise bounds for the approximation error associated with any computational algorithm applied to the Hemker problem. Here, we test for convergence of the numerical approximations using the double-mesh principle [13] and, more importantly, to identify when any numerical method fails to be convergent. We emphasize that we shall estimate the global pointwise convergence of the interpolated computed approximations across the entire domain. Numerical results with a preliminary version of this algorithm were reported in [14].

The Shishkin mesh [13,15] is a central component of the algorithm. The simplicity of this mesh is one of the key attributes of this particular layer-adapted mesh, which allows easy extensions to more complicated problems. Shishkin meshes have the additional property that, if one has established parameter-uniform nodal accuracy [13] in a subdomain, then (for problems with regular exponential boundary layers [16] and characteristic boundary layers [17]) this nodal accuracy extends to global accuracy across the subdomain using basic bi-linear interpolation. This interpolation feature of the mesh permits us employ overlapping subdomains, with different co-ordinate systems aligned to the local geometry of the layers, and to subsequently test computationally for global accuracy across the entire domain.

In [Section 2](#), we identify bounds on the solution of the Hemker problem restricted to a bounded domain. In [Section 3](#), we discuss how we computationally estimate the order of parameter-uniform convergence for any numerical method. In [Section 4](#), we construct and describe the numerical algorithm, which involves four distinct stages. The first two stages generate an initial approximation which has defects only near the characteristic points. The third and fourth stage correct this initial approximation. In [Section 5](#), we present numerical results to illustrate the performance of the final algorithm. The numerical results indicate that this new algorithm is generating numerical approximations which are converging, over an extensive range of the singular perturbation parameter, to the solution of a bounded-domain version of the original Hemker problem.

**Notation:** We will employ three distinct co-ordinate systems in this paper. A Cartesian co-ordinate system  $(x, y)$ , a polar co-ordinate system  $(r, \theta)$  and a particular parabolic co-ordinate system  $(s, t)$ . In each co-ordinate system, we adopt the following notation for functions:

$$f(x, y) = \hat{f}(s, t) = \tilde{f}(r, \theta).$$

We use these co-ordinate systems to solve various sub-problems on an annulus  $A$ , a rectangle  $S$  and planar regions  $Q^+, Q^-$ . The numerical solution is determined using four sub-components  $U_A, U_B, U_C$  and  $U_D$ ; where  $U_A$  is defined over the annulus  $A$ ,  $U_C$  is defined over the planar region  $Q^+ \cup Q^-$  and  $U_B, U_D$  are defined over the rectangular region  $S$ . In addition, the algorithm produces an initial global approximation  $\bar{U}_1^N$ , which is shown to lose accuracy in some of the layers. This initial approximation is subsequently corrected to produce a globally pointwise accurate approximation  $\bar{U}_2^N$ . Throughout the paper,  $\|\cdot\|_D$  denotes the supremum or maximum norm measured over the domain  $D$ .

## 2. The continuous problem

In this paper, we confine our discussion to the Hemker problem (1) posed on a bounded domain of dimension  $O(R^2)$ . Consider the singularly perturbed elliptic problem: Find  $u(x, y)$  such that

$$Lu := -\varepsilon \Delta u + u_x = 0, \quad (x, y) \in \Omega; \tag{2a}$$

$$u = 0, (x, y) \in \partial\Omega_0; \quad u_x = 0, (x, y) \in \partial\Omega_N; \quad u = 1, (x, y) \in \partial\Omega_I; \tag{2b}$$

where the bounded domain  $\Omega$  and the boundaries  $\partial\Omega_0, \partial\Omega_N, \partial\Omega_I$  are defined to be

$$\Omega := \{(x, y) | 1 < x^2 + y^2 < R^2, x \leq 0\} \cup \{(x, y) | -R < y < R, 0 < x < R, 1 < x^2 + y^2\}, \tag{2c}$$

$$\partial\Omega_N := \{(R, y) | -R < y < R\}, \quad \partial\Omega_I := \{(x, y) | x^2 + y^2 = 1\}; \tag{2d}$$

$$\partial\Omega_0 := \{(x, y) | x^2 + y^2 = R^2, x \leq 0\} \cup \{(x, y) | y = \pm R, 0 \leq x \leq R\}. \tag{2e}$$

A sample computed solution (using the algorithm (21)) is displayed in Fig. 1, which illustrates the location of the layers that can appear in the solution. In all of our numerical experiments, we have simply taken  $R = 4$ .

We have a minimum principle associated with this problem.

**Theorem 1** ([18, pg. 61]). *For any  $w \in C^0(\bar{D}) \cap C^2(D), D \subset \Omega$ , if  $Lw(x, y) \geq 0, (x, y) \in D$ , then  $\min_{\bar{D}} w \geq \min_{\partial D} w$ .*

**Proof.** Consider the special case of  $\min_{\partial D} w = 0$ . Assume  $w < 0$  at some internal point. Then the function  $v := e^{-\frac{x}{2\varepsilon}} w$  is negative at some interior point. However, then  $Lw = e^{\frac{x}{2\varepsilon}} (-\varepsilon \Delta v + \frac{1}{4\varepsilon} v) < 0$  at the point where  $v$  takes its minimum value. This is a contradiction. Complete the proof by considering the function  $w_1 := w - \min_{\partial D} w$ .  $\square$

Thus, we have a comparison principle.

**Corollary 1.** *If  $w, v \in C^0(\bar{D}) \cap C^2(D), D \subset \Omega$  are such that  $Lw(x, y) \geq Lv(x, y), \forall (x, y) \in D$  and  $w \geq v$  on the boundary  $\partial D$ , then  $w(x, y) \geq v(x, y), \forall (x, y) \in \bar{D}$ .*

For any open connected subdomain  $D \subset \Omega$  we define the boundaries

$$\partial D_N := \{\bar{p} \in \partial D | (1, 0) \cdot \bar{n}_p > 0\} \quad \text{and} \quad \partial D_0 := \partial D \setminus \partial D_N;$$

where  $\bar{n}_p$  is the outward normal to  $\partial D$  at  $\bar{p}$ . As in [18, pg.65], we can establish

**Theorem 2.** *If  $w, v \in C^0(\bar{D}) \cap C^2(D), D \subset \Omega$  are such that  $Lw(x, y) \geq Lv(x, y), \forall (x, y) \in D; w \geq v$  on the boundary  $\partial D_0$  and  $w_x \geq v_x$  on the boundary  $\partial D_N$ , then  $w(x, y) \geq v(x, y), \forall (x, y) \in \bar{D}$ .*

Let us partition the domain  $\Omega$  into a finite number of non-overlapping subdomains  $\{D_i\}_{i=1}^n$  such that

$$D_i \cap D_j = \emptyset, i \neq j, \quad \bar{\Omega} = \cup_{i=1}^n \bar{D}_i \quad \text{and} \quad \Gamma_{i,j} := \bar{D}_i \cap \bar{D}_j.$$

Let  $\frac{\partial u}{\partial n_i}$  denote the outward normal derivative of each subdomain  $D_i$  and

$$\left[ \frac{\partial u}{\partial n} \right]_{\Gamma_{i,j}} = \frac{\partial u}{\partial n_i} |_{\Gamma_{i,j}} + \frac{\partial u}{\partial n_j} |_{\Gamma_{i,j}}.$$

Using the usual proof by contradiction argument (with a separate argument for the interfaces  $\Gamma_{i,j}$ ) we can establish the following

**Theorem 3.** *If  $w, v \in C^0(\bar{\Omega}) \cap C^2(\cup_{i=1}^n D_i)$  is such that (a)  $Lw(x, y) \geq Lv(x, y), \forall (x, y) \in D_i$  for all  $i$ ; (b)  $\left[ \frac{\partial w}{\partial n} \right]_{\Gamma_{i,j}} \geq \left[ \frac{\partial v}{\partial n} \right]_{\Gamma_{i,j}}$  for all  $i, j$ ; (c)  $w \geq v$  on the boundary  $\partial\Omega_0$  and (d)  $w_x \geq v_x$  on the boundary  $\partial\Omega_N$ , then  $w(x, y) \geq v(x, y), \forall (x, y) \in \bar{\Omega}$ .*

**Proof.** Consider the function  $z := e^{-\frac{x}{2\varepsilon}} (w - v)$  and assume that  $z(\bar{p}) := \min_{\bar{\Omega}} z < 0$ . By (c),  $z$  is not a constant function and  $\bar{p} \notin \partial\Omega_0$ . Note that  $(w - v)_x = e^{\frac{x}{2\varepsilon}} (z_x + \frac{1}{2\varepsilon} z)$  and so, by (d),  $\bar{p} \notin \partial\Omega_N$ . By (a),  $\bar{p} \notin D_i$  for any  $i$ , as  $L(w - v) = e^{\frac{x}{2\varepsilon}} (-\varepsilon \Delta z + \frac{1}{4\varepsilon} z)$ . Finally,

$$\left[ \frac{\partial(w - v)}{\partial n} \right]_{\Gamma_{i,j}} = e^{\frac{x}{2\varepsilon}} \left[ \frac{\partial z}{\partial n} \right]_{\Gamma_{i,j}}$$

and, using the argument [18, Theorems 7 and 8, pp. 65–67] over each subdomain  $D_i$ , we have that  $\frac{\partial z}{\partial n}(\bar{p}) < 0$  if  $\bar{p} \in \Gamma_{i,j}$ . Hence we have the strict inequality  $\left[\frac{\partial z}{\partial n}\right]_{\Gamma_{i,j}}(\bar{p}) < 0$ , which contradicts (b).  $\square$

Using these results, we can establish the following bounds on the solution:

**Theorem 4.** *Assuming  $\varepsilon$  is sufficiently small, then the solution  $u$  of problem (2) satisfies the following bounds*

$$0 \leq u(x, y) \leq 1, \quad (x, y) \in \bar{\Omega}; \tag{3a}$$

$$\tilde{u}(r, \theta) \leq Ce^{\frac{\cos(\theta)(r-1)}{\varepsilon}}, \quad \cos \theta \leq 0, \quad r \geq 1; \tag{3b}$$

$$u(x, y) \leq Ce^{-\frac{|y-1|}{\sqrt{\varepsilon}}}, \quad |y| \geq 1, \quad -R < x < R; \tag{3c}$$

$$u(x, y) \leq Ce^{-\frac{(0.5x^2+|y-1|)}{3\varepsilon^{2/3}}}, \quad x \in \varepsilon^{1/3}[-1, 1], \quad -C\varepsilon^{2/3} \leq 0.5x^2 + |y| - 1 \leq C\varepsilon^{2/3}. \tag{3d}$$

**Proof.** The first bound follows easily from the minimum principle. See details in the appendix for all of the remaining bounds.  $\square$

### 3. Computationally testing for convergence

As identified in [1], we do not have a useable closed form representation of the exact solution to the Hemker problem to allow us to evaluate the accuracy of any computed approximation. The infinite series representation [1] for the exact solution has difficulties for moderately small values of the singular perturbation parameter  $\varepsilon$ . Hence, to test for convergence we rely on the double-mesh method of estimating the order of convergence [13, Chapter 8]. We elaborate on this experimental approach in this section.

For every particular value of  $\varepsilon$  and  $N$ , let  $U_\varepsilon^N$  be the computed solutions on certain meshes  $\Omega_\varepsilon^N$ , where  $N$  denotes the number of mesh elements used in each co-ordinate direction. Define the maximum local two-mesh global differences  $D_\varepsilon^N$  and the maximum parameter-uniform two-mesh global differences  $D^N$  by<sup>1</sup>

$$D_\varepsilon^N := \|\tilde{U}_\varepsilon^N - \tilde{U}_\varepsilon^{2N}\|_{\Omega_\varepsilon^N \cup \Omega_\varepsilon^{2N}} \quad \text{and} \quad D^N := \sup_{0 < \varepsilon \leq 1} D_\varepsilon^N,$$

where  $\tilde{U}_\varepsilon^N$  denotes the bilinear interpolation of the discrete solution  $U_\varepsilon^N$  on the mesh  $\Omega_\varepsilon^N$ . Then, for any particular value of  $\varepsilon$  and  $N$ , the local orders of global convergence are denoted by  $\bar{p}_\varepsilon^N$  and, for any particular value of  $N$  and *all values of  $\varepsilon$* , the **parameter-uniform** global orders of convergence  $\bar{p}^N$  are defined, respectively, by

$$\bar{p}_\varepsilon^N := \log_2 \left( \frac{D_\varepsilon^N}{D_\varepsilon^{2N}} \right) \quad \text{and} \quad \bar{p}^N := \log_2 \left( \frac{D^N}{D^{2N}} \right).$$

If, for a certain class  $\mathcal{C}$  of singularly perturbed problems, there exists a theoretical error bound of the form: There exists a constant  $C$  independent of  $\varepsilon$  and  $N$  such that for all  $\varepsilon > 0$

$$\|\tilde{U}^N - u\|_\Omega \leq CN^{-p}, \quad p > 0; \tag{4}$$

then it follows that

$$D^N \leq C(1 + 2^{-p})N^{-p}.$$

Hence, for any particular sample problem from this class  $\mathcal{C}$ , we expect to observe this theoretical convergence rate  $p$  in the computed rates of convergence  $\bar{p}^N$ . That is, we expect that  $\bar{p}^N \approx p$ .

A useful attribute of the two-mesh method is that we can use it to identify when a numerical method is not parameter-uniform. Observe that

$$\|\tilde{U}_\varepsilon^N - \tilde{U}_\varepsilon^{2N}\|_\Omega \leq \|\tilde{U}_\varepsilon^N - u\|_\Omega + \|u - \tilde{U}_\varepsilon^{2N}\|_\Omega.$$

Hence, if the parameter-uniform two mesh differences  $D^N$  fail to converge to zero, then the numerical method is also not a parameter-uniform numerical method. In our quest for a parameter-uniform numerical method, we used this feature to identify necessary components to construct a parameter-uniform numerical method. On the other hand, without the existence of a theoretical error bound (4) (as is the case with the Hemker problem), if the global two mesh differences  $D^N$  are seen to converge then we can only conclude that the numerical method may be a parameter-uniform numerical method. We would require a theoretical parameter-uniform error bound on the numerical approximations, before one can assert that the numerical method is indeed parameter-uniform.

For any numerical method applied to a class of singularly perturbed problems, our primary interest is in determining the parameter-uniform orders of global convergence  $\bar{p}^N$ . However, we can also examine the local orders of convergence

<sup>1</sup> In passing we note that, in general, for a piecewise-uniform Shishkin mesh  $\Omega_\varepsilon^N \cup \Omega_\varepsilon^{2N} \neq \Omega_\varepsilon^{2N}$ , as the transition point (where the mesh is not uniform) depends on  $N$ .

$\bar{p}_\varepsilon^N$  to see how the numerical method performs for each possible value of  $\varepsilon$  over the range  $0 < \varepsilon \leq 1$ . In general, we note that  $\bar{p}^N \neq \min_\varepsilon \bar{p}_\varepsilon^N$ . In the case of piecewise-uniform meshes, certain anomalies can sometimes be observed in the local orders of convergence (i.e.,  $\bar{p}_\varepsilon^N \not\approx \bar{p}^N$ ) for certain values of  $\varepsilon$ . We illustrate this effect with the following theoretical example. Based on the nature of the typical errors on a piecewise-uniform Shishkin mesh in a one dimensional convection–diffusion problem, suppose that the two-mesh differences  $D_\varepsilon^N$  were of the form

$$D_\varepsilon^N := \begin{cases} \frac{\rho}{1+\rho} & \text{if } k\varepsilon \ln N \geq 1 \\ N^{-1} & \text{if } k\varepsilon \ln N < 1 \end{cases}; \quad \text{where } \rho := \frac{1}{\varepsilon N}, \quad k \geq 1.$$

For this theoretical example, the parameter-uniform two mesh differences can be explicitly determined. Note first that

$$D_\varepsilon^N \leq \begin{cases} \frac{k \ln N}{N+k \ln N} & \text{if } k\varepsilon \ln N \geq 1 \\ N^{-1} & \text{if } k\varepsilon \ln N < 1 \end{cases}.$$

Hence, if  $N \geq 4, k \geq 1$ , we have

$$D^N = \frac{k \ln N}{N+k \ln N} \quad \text{and} \quad \lim_{N \rightarrow \infty} \bar{p}^N = 1.$$

Let us now consider the particular values of  $\varepsilon = 2^{-4}, k = 4$  and  $N = 32$ . First observe that

$$D_{\varepsilon=2^{-4}}^N = \begin{cases} \frac{\rho_*}{1+\rho_*} & \text{if } \ln N \geq 4 \\ N^{-1} & \text{if } \ln N < 4 \end{cases}, \quad \text{where } \rho_* = 16N^{-1}.$$

Then, in particular,

$$D_{\varepsilon=2^{-4}}^{32} = 2^{-5}, D_{\varepsilon=2^{-4}}^{64} = 0.2,$$

which yields the order of convergence as

$$\bar{p}_{\varepsilon=2^{-4}}^{32} \approx -2.68 \quad \text{although} \quad \bar{p}^{32} \approx 0.55.$$

Thus, we can have negative local orders of convergence  $\bar{p}_\varepsilon^N$ , for particular values of  $\varepsilon$  and  $N$  and still have positive parameter-uniform orders of convergence  $\bar{p}^N$ . This phenomena will appear in the numerical results section in Section 5.

In practice, note that the parameter-uniform orders  $\bar{p}^N$  can only be estimated over a finite set  $R_\varepsilon^J := \{2^{-j}, j = 0, 1, \dots, J\}$  of values of the singular perturbation parameter  $\varepsilon \in (0, 1]$ . That is, we define

$$\bar{p}_{R_\varepsilon^J}^N := \log_2 \left( \frac{D_{R_\varepsilon^J}^N}{D_{R_\varepsilon^J}^{2N}} \right), \quad \text{where} \quad D_{R_\varepsilon^J}^N := \max_{\varepsilon \in R_\varepsilon^J} D_\varepsilon^N.$$

When a method is known to be parameter-uniform,  $J$  is taken sufficiently large so  $\bar{p}_{R_\varepsilon^K}^N = \bar{p}_{R_\varepsilon^J}^N$ , for any  $K > J$  and  $\bar{p}_{R_\varepsilon^J}^N$  is taken to be the computed estimate of  $\bar{p}^N$ .

In this paper, we construct a numerical method that displays positive orders of convergence  $\bar{p}_{R_\varepsilon^{20}}^N$ , for  $N$  sufficiently large; i.e.,  $N \geq N_0$ , where  $N_0$  is independent of  $\varepsilon$ , when the numerical method is applied to the Hemker problem and the range of the singular perturbation parameter is  $\varepsilon \in R_\varepsilon := \{2^{-j}, j = 0, 1, \dots, 20\}$ . For smaller values of the parameter ( $\varepsilon < 2^{-24}$ ), we have observed a degradation in the local orders of convergence. Hence, we cannot claim that the numerical method described in this paper is parameter-uniform. This lack of convergence might be due to the presence of an unidentified singularity; but, in effect, the character of the solution for  $\varepsilon < 2^{-20}$  remains an open question.

To conclude this section, we note that the two-mesh differences are computed to enable the computation of approximate orders of convergence. To generate approximations to the pointwise errors for any particular value of  $N$  and  $\varepsilon$ , we compare the computed solution for a given number of mesh points  $N$  to the computed solution on a fine mesh. That is, we approximate the nodal error by

$$\|U_\varepsilon^N - u\|_{\Omega_\varepsilon^N} \approx \|U_\varepsilon^N - \bar{U}_\varepsilon^{4N_*}\|_{\Omega_\varepsilon^N}, \quad \text{for any } N \leq N_*;$$

and the global error by

$$\|\bar{U}_\varepsilon^N - u\|_\Omega \approx \|\bar{U}_\varepsilon^N - \bar{U}_\varepsilon^{4N_*}\|_{\Omega_\varepsilon^N \cup \Omega_\varepsilon^{4N_*}}, \quad \text{for any } N \leq N_*.$$

#### 4. The numerical algorithm

Polar coordinates are a natural co-ordinate system to employ in the semi-annular region to the left of the line  $x = 0$  and rectangular co-ordinates are natural to the right of the line  $x = 0$ . To incorporate both co-ordinate systems, we first generate an approximate solution to the problem (2) on the sector

$$\tilde{A} := \{(r, \theta) | 1 < r < R, \frac{\pi}{2} - \tau \leq \theta \leq \frac{3\pi}{2} + \tau\}, \tag{5}$$

which is a proper subset of the domain  $\Omega$  and the parameter  $\tau$  is specified below in (7b).

The continuous problem (2), restricted to the sector  $\tilde{A}$ , is transformed into the problem: Find a periodic function,  $\tilde{u}(r, \theta) = u(x, y)$  such that

$$\tilde{L}\tilde{u} := -\frac{\varepsilon}{r^2}\tilde{u}_{\theta\theta} - \varepsilon\tilde{u}_{rr} + (\cos(\theta) - \frac{\varepsilon}{r})\tilde{u}_r - \frac{\sin(\theta)}{r}\tilde{u}_\theta = 0, \text{ in } \tilde{A}; \tag{6a}$$

$$\tilde{u}(1, \theta) = 1, \quad \frac{\pi}{2} - \tau \leq \theta \leq \frac{3\pi}{2} + \tau; \quad \tilde{u}(R, \theta) = 0, \quad \frac{\pi}{2} \leq \theta \leq \frac{3\pi}{2}. \tag{6b}$$

The remaining boundary points of this sector  $\tilde{A}$  are internal points within the domain  $\Omega$ , where the discrete solution has not yet been specified. In order to generate an initial approximation to the solution  $\tilde{u}$ , we impose homogeneous Neumann conditions at these internal points of the form:

$$u_x^A(x, y) = 0, \text{ if } x^2 + y^2 = R^2 \text{ and } x > 0; \tag{6c}$$

$$\tilde{u}_\theta^A(r, \frac{\pi}{2} - \tau) = \tilde{u}_\theta^A(r, \frac{3\pi}{2} + \tau) = 0, \text{ for } 1 < r < R, \tag{6d}$$

where  $u^A(x, y) \approx u(x, y)$  for  $x \leq 0$ .

**Remark 1.** The choice of a homogeneous Neumann condition at the outflow is motivated by the following observation: Consider the one-dimensional convection–diffusion problem: Find  $z(x), x \in [0, L]$  such that

$$-\varepsilon z'' + az' = f(x), \quad x \in (0, L); \quad z(0) = A, z(L) = B; \quad a(x) \geq \alpha > 0$$

and the approximate problem: Find  $z_A(x), x \in [0, L]$  such that

$$-\varepsilon z_A'' + az_A' = f(x), \quad x \in (0, L); \quad z_A(0) = z(0), z_A'(L) = 0.$$

Using a comparison principle (as in Theorem 2), we can establish the bound

$$|(z - z_A)(x)| \leq \frac{\varepsilon|z'(L)|}{\alpha} e^{-\frac{\alpha(L-x)}{\varepsilon}}.$$

Hence,  $z_A$  is an  $O(N^{-1})$ -approximation to  $z$ , at some  $O(\varepsilon \ln N)$  distance away from the end-point  $x = L$ . That is:

$$|(z - z_A)(x)| \leq C\varepsilon|z'(L)|N^{-1} \leq CN^{-1}; \quad \text{if } x \in [0, L - \frac{\varepsilon \ln N}{\alpha}].$$

This problem (6) is discretized using simple upwinding on a tensor product piecewise-uniform Shishkin mesh, whose construction is motivated by the bounds (3b), (3d). Two transition points (where the mesh step changes in magnitude) are used in the radial direction. The choice of the first transition point  $\sigma_1$  is motivated by considering the bound (3b) at some fixed distance  $x < -\delta < 0$  to the left of  $x = 0$  and by the theoretical error bounds [19] established for this mesh in the region where  $x < -\delta < 0$ . The choice of this point  $x = -\delta$  is arbitrary. As in [19], we simply take it to correspond to a critical angle  $\theta_*$ , such that

$$\kappa \cos \theta_* = -\frac{1}{2}, \quad 0.5 < \kappa \leq 1,$$

where  $\kappa$  is again arbitrary. Hence, we have that

$$\tilde{u}(r, \theta) \leq Ce^{-\frac{r-1}{2\varepsilon}}, \quad \text{for } \theta_* \leq \theta \leq 2\pi - \theta_*$$

and

$$\tilde{u}(r, \theta) \leq CN^{-1}, \quad \text{if } r \geq 1 + 2\varepsilon \ln N \text{ and } \theta_* \leq \theta \leq 2\pi - \theta_*.$$

A second transition point  $\sigma_2$  is motivated by the bound (3d) applied along the line  $x = 0$ . In the angular direction, the bound (3d) also motivates the inclusion of a transition point  $\tau$  in the vicinity of the characteristic points. See also [9, pg. 269], [10, pg. 188] and [11, pg. 1183] for motivation for these scales in the vicinity of the characteristic points  $(0, \pm 1)$ .

**The Shishkin mesh**  $\tilde{\Omega}_A^N$  The radial domain  $[1, R]$  is divided into three subregions. The radii  $r = 1, r = 1 + \sigma_1, r = 1 + \sigma_1 + \sigma_2, r = R$ , mark the subregion boundaries and the radial transition points are taken to be

$$\sigma_1 := \min\{\frac{R-1}{4}, 2\varepsilon \ln N\} \quad \text{and} \quad \sigma_2 := \min\{\frac{R-1}{4}, 3\varepsilon^{2/3} \ln N\}. \tag{7a}$$

The  $N$  radial mesh points are distributed in the ratio  $N/4 : N/4 : N/2$  across these three subintervals. For the angular coordinate, the interval  $[\frac{\pi}{2} - \tau, \frac{3\pi}{2} + \tau]$  is split into three subintervals with the start/end points of each subinterval, respectively, at

$$\frac{\pi}{2} - \tau, \quad \frac{\pi}{2} + \tau, \quad \frac{3\pi}{2} - \tau, \quad \frac{3\pi}{2} + \tau$$

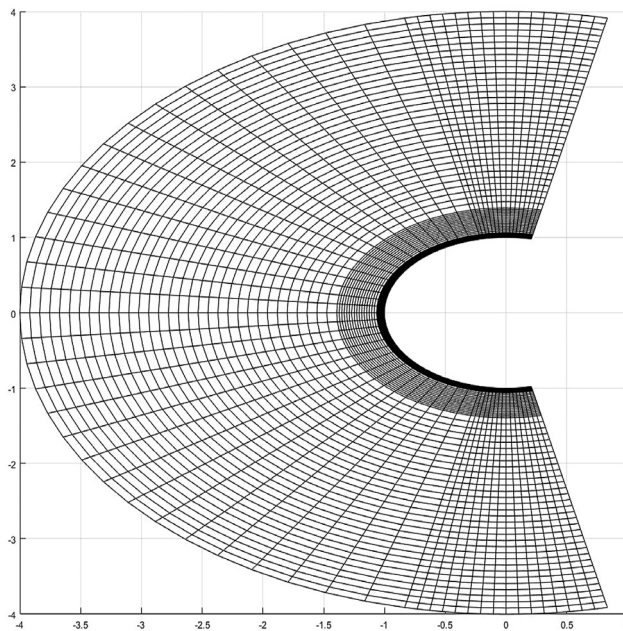


Fig. 2. A schematic image of the mesh  $\tilde{\Omega}_A^N$  (7) on the annular subregion  $\tilde{A}$  (5).

and the mesh points are distributed in the ratio  $N/4 : N/2 : N/4$  across the three associated subintervals. The transition points are determined by

$$\tau := \min\left\{\frac{\pi}{6}, \sqrt{6}\varepsilon^{1/3} \ln N\right\}. \tag{7b}$$

A schematic image of this mesh is presented in Fig. 2. However, in practice, the refinement in the radial direction only becomes apparent to the user for very small values of  $\varepsilon$ .

At the mesh points on the sector  $\tilde{A}$ , the computed solution will (in polar coordinates) be denoted by  $U_A(r_i, \theta_j)$ ,  $(r_i, \theta_j) \in \tilde{\Omega}_A^N$ . This approximation is extended to the global approximation  $\tilde{U}_A(r, \theta)$ ,  $(r, \theta) \in \tilde{A}$ , using simple bilinear interpolation<sup>2</sup>. We will utilize the following finite difference operators  $D_r^+$ ,  $D_r^-$ ,  $D_r^\pm$ ,  $\delta_r^2$  defined by

$$D_r^+ Z(r_i, \theta_j) := \frac{Z(r_{i+1}, \theta_j) - Z(r_i, \theta_j)}{r_{i+1} - r_i}, \quad D_r^- Z(r_i, \theta_j) := \frac{Z(r_i, \theta_j) - Z(r_{i-1}, \theta_j)}{r_i - r_{i-1}};$$

$$2(bD_r^\pm)Z := (b - |b|)D_r^+ Z + (b + |b|)D_r^- Z; \quad \delta_r^2 Z(r_i, \theta_j) := \frac{D_r^+ Z(r_i, \theta_j) - D_r^- Z(r_i, \theta_j)}{(r_{i+1} - r_{i-1})/2}.$$

**Stage 1: Numerical method for  $U_A$  defined over an annular subregion  $\tilde{A}$**

Find  $U_A$  such that:

$$\tilde{L}^N U_A = 0, \quad (r_i, \theta_j) \in \Omega_A^N; \tag{8a}$$

$$\text{where } \tilde{L}^N U := -\frac{\varepsilon}{r_i^2} \delta_\theta^2 U - \varepsilon \delta_r^2 U + (\cos(\theta_j) - \frac{\varepsilon}{r_i}) D_r^\pm U - \frac{\sin(\theta_j)}{r_i} D_\theta^\pm U; \tag{8b}$$

$$U_A(1, \theta_j) = 1, \quad \frac{\pi}{2} - \tau \leq \theta_j \leq \frac{3\pi}{2} + \tau; \quad U_A(R, \theta_j) = 0, \quad \frac{\pi}{2} \leq \theta_j \leq \frac{3\pi}{2}; \tag{8c}$$

$$(\cos \theta D_r^- - \frac{\sin \theta}{R} D_\theta^\pm) U_A(R, \theta_j) = 0, \quad \theta_j \in (\frac{\pi}{2} - \tau, \frac{\pi}{2}) \cup (\frac{3\pi}{2}, \frac{3\pi}{2} + \tau); \tag{8d}$$

<sup>2</sup> Over any computational cell  $\Omega_{i,j} := (x_{i-1}, x_i) \times (y_{j-1}, y_j)$ , where  $h_i := x_i - x_{i-1}$ ,  $k_j := y_j - y_{j-1}$ , we denote the bilinear interpolant of any function  $g(x, y)$  by  $\tilde{g}$ . For any smooth function  $v$ , where  $\|v_{xx}\|_{\Omega_{i,j}} + \|v_{yy}\|_{\Omega_{i,j}} \leq C$ , then  $\|v - \tilde{v}\|_{\Omega_{i,j}} \leq Ch_i^2 + Ck_j^2$ . For a layer function of the form  $w(x, y) = e^{-\alpha x/\varepsilon^p}$ ,

$$\|w - \tilde{w}\|_{\Omega_{i,j}} \leq C\|w\|_{\Omega_{i,j}} \leq CN^{-1}, \quad \text{if } x_i \geq \frac{\varepsilon^p \ln N}{\alpha}, \quad \text{and}$$

$$\|w - \tilde{w}\|_{\Omega_{i,j}} \leq Ch_i \|w_x\|_{\Omega_{i,j}} \leq CN^{-1} \ln N, \quad \text{if } h_i \leq C\varepsilon^p N^{-1} \ln N.$$

**Table 1**

Computed double-mesh global orders of convergence  $\bar{p}_\varepsilon^N$  using the mesh  $\bar{\Omega}_A^N$  (7) with  $x \leq 0$ , when applied to problem (2) confined to the sector  $\bar{A}$  with  $R = 4$ .

$\bar{p}_\varepsilon^N$							
$\varepsilon N$	N=8	16	32	64	128	256	512
$\varepsilon = 1$	0.9855	0.9966	0.9996	0.9996	1.0002	1.0001	1.0000
$2^{-2}$	1.0014	0.9115	0.9643	0.9867	0.9918	0.9958	0.9979
$2^{-4}$	0.4693	0.6789	0.7825	0.6875	0.6950	0.7541	0.9911
$2^{-6}$	0.5832	0.7176	0.7760	0.6887	0.7691	0.7990	0.8255
$2^{-8}$	0.7205	0.7771	0.8441	0.6893	0.7713	0.7991	0.8266
$2^{-10}$	0.3249	0.7079	0.9677	0.8376	0.9761	0.9231	0.8270
$2^{-12}$	0.1131	0.4659	0.8732	0.9145	0.8086	0.9597	1.0268
$2^{-14}$	0.1242	0.5344	0.6122	0.7242	0.8605	0.7995	0.9612
$2^{-16}$	0.1669	0.4506	0.4704	0.6033	0.7562	0.8573	0.8242
$2^{-18}$	0.2113	0.2972	0.3714	0.5046	0.6604	0.7978	0.8561
$2^{-20}$	0.2111	0.1873	0.2770	0.4167	0.5625	0.7077	0.8373
$\bar{p}_{R\varepsilon}^N$	0.2111	0.1873	0.2770	0.4167	0.5625	0.7077	0.8373

$$D_\theta^+ U^A(r_i, \frac{\pi}{2} - \tau) = D_\theta^- U^A(r_i, \frac{3\pi}{2} + \tau) = 0, \quad \text{for } 1 < r_i < R. \tag{8e}$$

The boundary condition ((8)d) corresponds to applying the Neumann condition  $u_x = 0$  at these internal points of  $\bar{\Omega}$ .

In Table 1, we present the results from applying this numerical method to problem (2) posed on the sector  $A \subset \Omega$ . We display the orders of convergence only for the region where  $x \leq 0$  and we observe global convergence over the parameter range  $\varepsilon \in [2^{-20}, 1]$ .

We next introduce a rectangular mesh, which will be aligned to the internal characteristic layers. We retain the computed solution  $\bar{U}_A$  in the upwind region where  $x \leq 0$  and then solve the problem (2) over the remaining rectangle

$$S := \{(x, y) | 0 < x \leq R, -R \leq y \leq R\}, \tag{9}$$

using a piecewise-uniform mesh  $\Omega_S^N$ , whose transition parameters are related to the bounds (3c) on the continuous solution  $u$ . By (3c),

$$u(x, y) \leq CN^{-1}, \quad \text{if } y \geq 1 + 2\varepsilon^{1/2} \ln N.$$

**The Shishkin mesh**  $\Omega_S^N$  The mesh  $\Omega_S^N := \omega_u \times \omega_3$  is a tensor product mesh of a uniform mesh  $\omega_u$  in the horizontal direction and a Shishkin mesh  $\omega_3$ , which refines in the region of the interior characteristic layers. The mesh  $\omega_3$  is generated by splitting the vertical interval  $[-R, R]$  into the five subregions

$$[-R, -1 - \tau_2] \cup [-1 - \tau_2, -1 + \tau_1] \cup [-1 + \tau_1, 1 - \tau_1] \cup [1 - \tau_1, 1 + \tau_2] \cup [1 + \tau_2, R], \tag{10a}$$

distributing the mesh elements in the ratio  $N/8 : N/4 : N/4 : N/4 : N/8$  and

$$\tau_1 := \min\{\frac{1}{2}, 2\varepsilon^{1/2} \ln N\}; \quad \tau_2 := \min\{\frac{R-1}{2}, 2\varepsilon^{1/2} \ln N\}. \tag{10b}$$

Observe that some of the mesh points in  $\Omega_S^N$  lie within the unit circle, where the value of the continuous solution is known. See Fig. 3 for a schematic image of the composite mesh  $(\bar{\Omega}_A^N \cup \Omega_S^N) \setminus C_1$ .

**Stage 2: Numerical method for  $U_B$  defined over the downwind region  $S$ :**

Find  $U_B(x_i, y_j)$  such that

$$L^{N,M} U_B := \left(-\varepsilon \delta_x^2 - \varepsilon \delta_y^2 + D_x^-\right) U_B(x_i, y_j) = 0, \quad (x_i, y_j) \in \Omega_S^N \setminus C_1; \tag{11a}$$

$$U_B(x_i, y_j) \equiv 1, \quad (x_i, y_j) \in \Omega_S^N \cap C_1; \quad C_1 := \{(x, y) | x^2 + y^2 \leq 1\}; \tag{11b}$$

with the remaining boundary values computed from the equations

$$D_x^- U_B(R, y_j) = 0, \quad -R < y_j < R, \quad U_B(x_i, -R) = U_B(x_i, R) = 0, \quad x_i \in [0, R]; \tag{11c}$$

$$U_B(0, y_j) = \bar{U}_A(0, y_j), \quad y_j \in (-R, R) \setminus [-1, 1]. \tag{11d}$$

Here  $\bar{U}_A(0, y_j)$  is a linear interpolant of the values  $U_A(r_i, \theta_j)$  along the line  $x = 0$ .

The initial computed global approximation  $\bar{U}_1^N$  to the solution of problem (2) is:

$$\bar{U}_1^N(x, y) := \begin{cases} \bar{U}_A(r, \theta), & \text{for } (r, \theta) \in \bar{A} \setminus \{x \geq 0\} \\ \bar{U}_B(x, y), & \text{for } (x, y) \in S \setminus C_1, \end{cases} \tag{12}$$

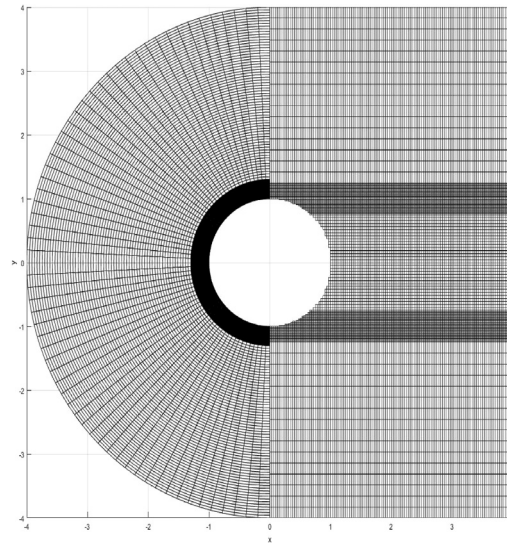


Fig. 3. A schematic image of the composite mesh  $(\tilde{\Omega}_A^N \cup \Omega_S^N) \setminus C_1$ , defined by (7) and (10).

Table 2

Computed double-mesh global orders of uniform convergence  $\bar{p}_\epsilon^N$ , for the mesh  $\tilde{\Omega}_A^N$  (7) used up to  $x = 0$  and subsequently combined with the rectangular mesh  $\Omega_S^N$  (10).

$\bar{p}_\epsilon^N$							
$N$	8	16	32	64	128	256	512
$\epsilon = 1$	1.1831	0.5014	0.7157	0.7719	0.8259	0.8743	0.9100
$2^{-2}$	1.7592	0.0305	0.4492	0.6880	0.7791	0.8460	0.8944
$2^{-4}$	1.0764	1.0413	0.0241	0.4368	0.6719	0.7768	0.8486
$2^{-6}$	0.2376	0.7503	1.7967	-0.9041	0.7151	0.4173	0.7648
$2^{-8}$	-0.0726	0.3699	0.6842	0.1372	0.8439	-0.0165	0.6041
$2^{-10}$	-0.0700	0.0504	0.4604	1.0622	0.4357	0.2011	0.4706
$2^{-12}$	-0.1139	-0.0051	0.2692	0.8506	1.0414	-0.0081	0.3631
$2^{-14}$	-0.1508	-0.0405	0.1558	0.5954	1.2268	0.1912	0.2453
$2^{-16}$	-0.1680	-0.0685	0.0477	0.3999	1.0007	0.7912	0.0780
$2^{-18}$	-0.1686	-0.0873	-0.0159	0.2119	0.7662	1.3778	-0.0380
$2^{-20}$	-0.1690	-0.0922	-0.0467	0.0795	0.5156	1.2055	0.5538

where  $U_A$  is defined by (8) and  $U_B$  is defined by (11).

In Table 2, we do not observe convergence of these initial numerical approximations  $\bar{U}_1^N$ . Hence, although we observe convergence in the annulus up to  $x \leq 0$ , this does not suffice to generate convergence across the entire domain, even if the mesh is fitted to the characteristic layers. In Figs. 4, 5 we plot the error across the entire domain and we observe a spike in the global pointwise error in the vicinity of the characteristic points. This global error does not decrease when the mesh is refined.

We next describe the construction of a correction  $\bar{U}_2^N$  to the initial approximation  $\bar{U}_1^N$ .

Let us return to the bounds on the continuous solution given in Theorem 4. From (3d), the bound on the solution remains constant along the parabolic path  $y - 1 = -\frac{1}{2}x^2$ . This is the motivation to introduce a third co-ordinate system that is aligned to these parabolic curves. Under this transformation, a mixed derivative term will appear in the transformed elliptic operator and we are required to restrict the dimensions of the sub-domain (where this new transformation is utilized) in order to preserve inverse-monotonicity of the corresponding discrete operator.

We introduce a patched region  $Q := Q^+ \cup Q^-$ , in a neighborhood of the vertical line  $x = 0$ . We discuss the approach on the upper region

$$Q^+ := \{(x, y) | y = t - x^2/2, \quad 0 < x < L < 1, \quad 1 - \tau_3 < t < 1 + 3\delta\}; \tag{13}$$

with an analogous definition of the lower region  $Q^-$ . The width  $L$  and height  $3\delta + \tau_3$  of this strip will be specified later in order to retain stability of the discrete operator.

A natural coordinate system for this patched region  $Q^+$  is

$$s = x, \quad t = y + x^2/2, \quad (y = t - s^2/2).$$

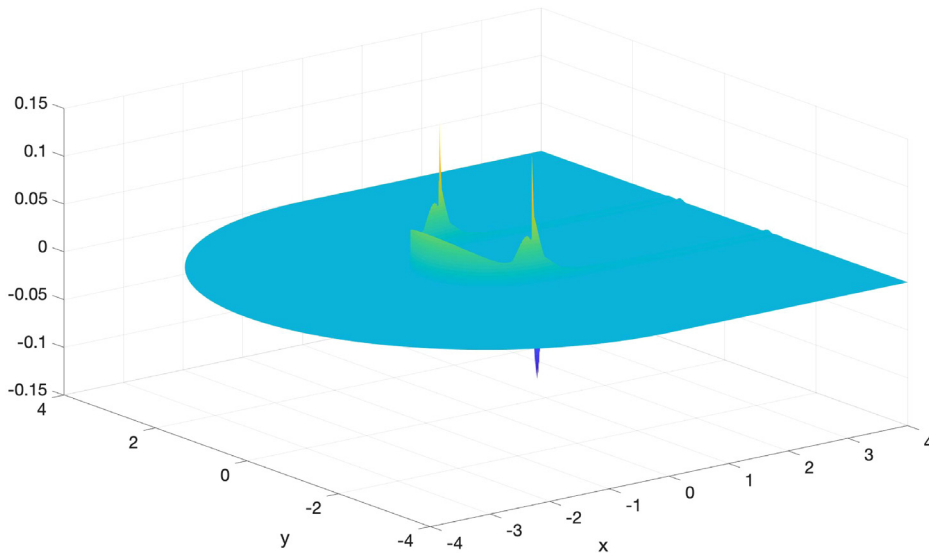


Fig. 4. Approximate global error  $\bar{U}_1^{128} - \bar{U}_1^{2048}$  on the mesh  $\tilde{\Omega}_A^N \cup \Omega_S^N$ , (7) and (10) with  $N = 2048$ , for  $\varepsilon = 2^{-10}$ .

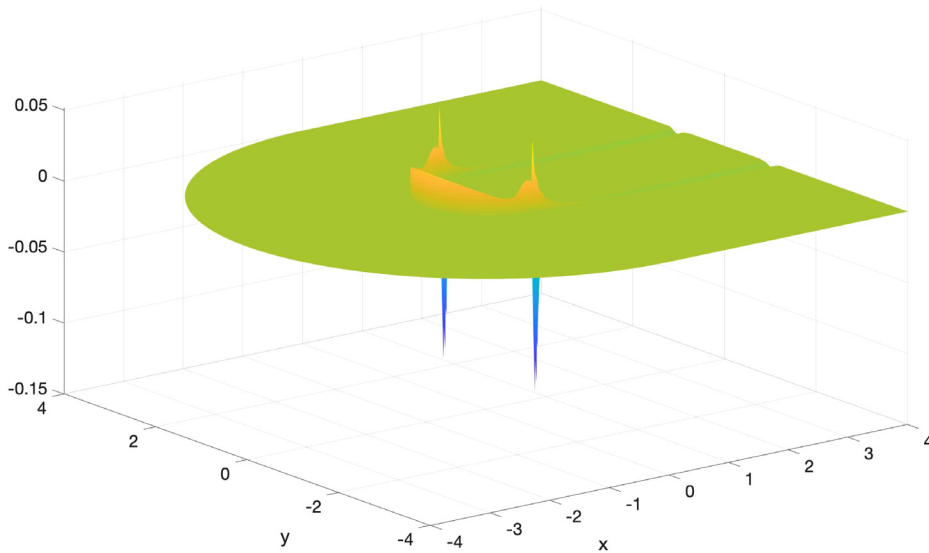


Fig. 5. Approximate global error  $\bar{U}_1^{256} - \bar{U}_1^{2048}$  on the mesh  $\tilde{\Omega}_A^N \cup \Omega_S^N$ , (7) and (10) with  $N = 2048$ , for  $\varepsilon = 2^{-10}$ .

Then let  $\hat{u}(s, t) := u(x, y)$ ,  $\hat{Q}^+ := (0, L) \times (1 - \tau_3, 1 + 3\delta)$  and

$$u_x = \hat{u}_s + s\hat{u}_t, \quad u_y = \hat{u}_t, \quad u_{yy} = \hat{u}_{tt}, \quad u_{xx} = \hat{u}_{ss} + 2s\hat{u}_{ts} + s^2\hat{u}_{tt} + \hat{u}_t.$$

Under this transformation the problem (2) on the patched region can be specified as follows

$$-\varepsilon(\hat{u}_{ss} + 2s\hat{u}_{ts} + (1 + s^2)\hat{u}_{tt}) + \hat{u}_s + (s - \varepsilon)\hat{u}_t = 0, \quad (s, t) \in \overline{\hat{Q}^+} \setminus C_1;$$

$$\hat{u}(s, t) = 1, \quad \text{if } s^2 + (t - s^2/2)^2 \leq 1.$$

We will use the initial computed approximation  $U_1^N$  (12) as boundary values to solve on the patched region  $\hat{Q}^+$  as follows:

$$\hat{L}\hat{u} := -\varepsilon(\hat{u}_{ss} + 2s\hat{u}_{ts} + (1 + s^2)\hat{u}_{tt}) + \hat{u}_s + (s - \varepsilon)\hat{u}_t = 0, \quad (s, t) \in \hat{Q}^+ \setminus C_1,$$

$$\hat{u}(s, 1 - \tau_3) = 1, \quad \hat{u}(s, 1 + 3\delta) = \bar{U}_1(s, 1 + 3\delta), \quad s \in (0, L),$$

$$\hat{u}(0, t) = \bar{U}_1(0, t), \quad \hat{u}_s(L, t) = 0, \quad t \in [1 - \tau_3, 1 + 3\delta],$$

$$\hat{u}(s, t) = 1, \quad \text{if } s^2 + (t - s^2/2)^2 \leq 1.$$

We again note the use of a Neumann boundary condition at the artificial internal boundary  $s = L$ . To ensure that the corner point  $(L, 1 - \tau_3)$  of this patch  $Q^+$  lies within the inner boundary ( $r < 1$ ) of problem (2), we require that

$$-\frac{1}{2}L^2 + 1 - \tau_3 < \sqrt{1 - L^2};$$

which, in turn, requires that

$$\tau_3 > \frac{L^2}{2} \frac{1 - \sqrt{1 - L^2}}{1 + \sqrt{1 - L^2}} = \frac{(1 - \sqrt{1 - L^2})^2}{2}. \tag{14}$$

We now specify the next phase of our numerical algorithm, where we correct the initial approximation  $\bar{U}_1$ .

We numerically solve the problem on the patch  $\hat{Q}^+$ , in the  $s, t$  coordinate system, using a Shishkin mesh  $\hat{\Omega}_p^{N,M}$  with two transition points located at  $t = 1 + \tau_3$  and  $1 + \tau_3 + \tau_4$ . The choice for the transition parameters  $\tau_3, \tau_4$  is motivated by the bounds (3c) and (3d), written in the  $(s, t)$  coordinates

$$\hat{u}(s, t) \leq C \min\{e^{-\frac{t-1}{3\varepsilon^{2/3}}}, e^{-\frac{t-1}{\sqrt{\varepsilon}}}\}, \quad \text{for } s \in \varepsilon^{1/3}[-1, 1].$$

**The Shishkin mesh  $\hat{\Omega}_p^{N,M}$**  We use a uniform mesh in the  $s$ -direction and a Shishkin mesh in the  $t$ -direction. The vertical strip  $[1 - \tau_3, 1 + 3\delta]$  is split into the following four sub-regions

$$[1 - \tau_3, 1] \cup [1, 1 + \tau_3] \cup [1 + \tau_3, 1 + (\tau_3 + \tau_4)] \cup [1 + (\tau_3 + \tau_4), 1 + 3\delta]$$

where

$$\tau_3 := \min\{\delta, 3\varepsilon^{2/3} \ln M\}, \quad \tau_4 := \min\{\delta, 2\sqrt{\varepsilon} \ln M\}, \tag{15}$$

and  $M/4$  mesh elements are distributed uniformly within each of these sub-intervals.

Within this patched region, we adopt the following notation

$$h = N^{-1}L, \quad k \leq k_j := t_j - t_{j-1} \leq K; \quad 2\bar{k}_j = k_j + k_{j+1},$$

where, as  $\tau_3 \leq \tau_4$ , we have

$$4M^{-1}\tau_3 \leq k \leq K \leq 12\delta M^{-1}.$$

Note that if we assume that

$$12\delta \leq MN^{-1}, \tag{16}$$

then the maximum mesh step  $K$  in the vertical direction will be such that  $K \leq N^{-1}$ .

**Stage 3: Numerical method for  $U_C$  defined near the characteristic points**

Find  $U_C$  such that:

$$\hat{L}^{N,M} \hat{U}_C := -\varepsilon \mathcal{L}^{N,M} \hat{U}_C + D_s^- \hat{U}_C + (s_i - \varepsilon) D_t^+ \hat{U}_C = 0, \quad (s_i, t_j) \in \hat{\Omega}_p^{N,M}; \tag{17a}$$

$$\text{where } \mathcal{L}^{N,M} Y := \delta_{ss}^2 Y + 2s\delta_{st} Y + (1 + s^2)\delta_{tt}^2 Y; \quad 2\delta_{st} := D_t^- D_s^- + D_t^+ D_s^+ \tag{17b}$$

and for the remaining mesh points

$$\hat{U}_C(0, t_j) = \bar{U}_1(0, t_j), \quad D_s^- \hat{U}_C(L, t_j) = 0, \quad 1 - \tau_3 \leq t_j \leq 1 + 3\delta; \tag{17c}$$

$$\hat{U}_C(s_i, 1 - \tau_3) = 1, \quad \hat{U}_C(s_i, 1 + 3\delta) = \bar{U}_1(s_i, 1 + 3\delta), \quad 0 < s_i < L; \tag{17d}$$

$$\hat{U}_C(s_i, t_j) = 1, \quad \text{if } s_i^2 + (t_j - s_i^2/2)^2 \leq 1. \tag{17e}$$

The presence of the mixed derivative term  $\varepsilon \hat{u}_{st}$  in the transformed problem, creates the danger of loss of stability in the discretization of the differential operator  $\hat{L}$  [20]. However, by restricting the dimensions of this parabolic patch, we are able to preserve an appropriate sign pattern in the system matrix elements, so that the matrix  $\mathcal{L}^{N,M}$  is an  $M$ -matrix.

**Theorem 5.** If we choose the dimension of the patch  $\hat{Q}^+$  (13) to satisfy

$$L \leq L_* := 2\sqrt{NM^{-1}\tau_3} \quad \text{and} \quad 12\delta \leq MN^{-1} \tag{18}$$

then the finite difference operator  $\hat{L}^{N,M}$  (17) satisfies a discrete comparison principle. That is, for any mesh function  $Z$ ,

$$\text{if } Z(s_i, 1 - \tau_1) \geq 0, Z(s_i, 1 + 3\delta) \geq 0, Z(0, t_j) \geq 0, \quad D_s^- Z(L, t_j) \geq 0, \quad \forall (s_i, t_j) \in \bar{Q}^+$$

$$\text{and } \hat{L}^{N,M} Z(s_i, t_j) \geq 0, \quad \forall (s_i, t_j) \in Q^+,$$

then  $Z(s_i, t_j) \geq 0, \quad \forall (s_i, t_j) \in \bar{Q}^+.$

**Proof.** Let us examine the sign patterns of the second order operator  $\mathcal{L}^{N,M}$  (defined in (17b)). From assumption (16), we have that

$$1 - \frac{\bar{k}_j s_i}{h} \geq 1 - \frac{KL}{h} \geq 1 - \frac{K}{2N} \geq 0.$$

Using this, we see that for the internal mesh points

$$-\mathcal{L}^{N,M} Y(s_i, t_j) = \sum_{n=j-1}^{j+1} \sum_{k=i-1}^{i+1} a_{kn} Y(s_k, t_n);$$

where the sign of most of the coefficients  $a_{kn}$  is easily identified to be

$$\begin{aligned} a_{i+1,j-1} = a_{i-1,j+1} = 0; \quad a_{i-1,j-1} = -\frac{s_i}{k_j h} \leq 0; \quad a_{i+1,j+1} = -\frac{s_i}{k_{j+1} h} \leq 0; \\ a_{i,j} = \frac{2}{h^2} + \frac{2}{k_j k_{j+1}} (1 + s_i^2 - \frac{\bar{k}_j |s_i|}{h}) > 0; \\ a_{i,j-1} = -\frac{(1 + s_i^2)}{\bar{k}_j k_j} + \frac{s_i}{k_j h} = -\frac{1}{\bar{k}_j k_j} (1 - \frac{\bar{k}_j s_i}{h} + s_i^2) < 0; \quad a_{i,j+1} = -\frac{(1 + s_i^2)}{k_j k_{j+1}} + \frac{s_i}{h k_{j+1}} < 0. \end{aligned}$$

Finally, we look at the last two terms,

$$a_{i-1,j} = a_{i+1,j} = -\frac{1}{h^2} + \frac{s_i}{h k_j}, \quad a_{i+1,j} = -\frac{1}{h^2} + \frac{s_i}{h k_{j+1}}.$$

Observe that

$$\max\{a_{i-1,j}, a_{i+1,j}\} \leq -\frac{1}{h^2} (1 - \frac{Lh}{k}) \leq -\frac{1}{h^2} (1 - \frac{ML^2}{4N\tau_3}) \leq 0,$$

if we choose  $L$  such that (18) is satisfied. This sign pattern on the matrix elements insures that the system matrix associated with the finite difference scheme is an M-matrix [13, pg.19], which suffices to establish the result.  $\square$

The constraints in (14) and (18) are all satisfied if

$$M = N, \quad L^2 = 4\tau_3 \quad \text{and} \quad \tau_3 \leq \delta \leq \frac{1}{12},$$

as  $2x > (1 - \sqrt{1 - 4x})^2$  for  $0 < x < \frac{2}{9}$ .

In the final phase, we solve the following discrete problem over the rectangle

$$S^* := (L_*, R) \times (-R, R) \subset S, \quad L_* := 2\sqrt{NM^{-1}\tau_3}; \tag{19}$$

using the mesh  $\Omega_S^N$ , which was defined in (10).

**Stage 4: Numerical method for  $U_D$  defined over the downwind region  $S^*$**

Find  $U_D$  such that

$$L^{N,M} U_D(x_i, y_j) = 0, \quad (x_i, y_j) \in \Omega_S^N \setminus \bar{C}_1; \tag{20a}$$

$$U_D(L_*, y_j) = \begin{cases} \bar{U}_C(L_*, y_j), & y_j \in (-1 - 3\delta, 1 + 3\delta); \\ \bar{U}_1(L_*, y_j), & y_j \in [-R, -1 - 3\delta] \cup [1 + 3\delta, R], \quad \delta \leq M/(12N); \end{cases} \tag{20b}$$

$$D_x^- U_D(R, y_j) = 0, \quad -R < y_j < R, \quad U_D(x_i, -R) = U_D(x_i, R) = 0, \quad x_i \in [L_*, R]. \tag{20c}$$

Then our corrected numerical approximation is given by

$$\bar{U}_2^N(x, y) := \begin{cases} \bar{U}_1(x, y), & \text{for } (x, y) \in \bar{\Omega} \setminus (\{x \geq L^*\} \cup Q^+ \cup Q^-) \\ \bar{U}_C(x, y), & \text{for } (x, y) \in Q^+ \cup Q^-, \\ \bar{U}_D(x, y), & \text{for } (x, y) \in (\{x \geq L^*\} \cap \Omega) \setminus (Q^+ \cup Q^-) \end{cases}. \tag{21}$$

In the next section, we present some numerical results to illustrate the convergence properties of this corrected approximation, which is defined across three different coordinate systems. A schematic image of the composite mesh  $\hat{\Omega}_A^{N,M} \cup \hat{\Omega}_P^{N,M} \cup \Omega_S^{N,M}$  is presented in Fig. 6.

### 5. Numerical results

In the previous section, we have seen that the initial approximations  $\bar{U}_1^N$  displayed a lack of convergence, due to the presence of large errors in the neighborhood of the characteristic points. The corrected approximations  $\bar{U}_2^N$  incorporate a parabolic patch near these points. In the numerical experiments in this section, we have taken  $M = N$ ,  $\delta = 0.05$  and, for

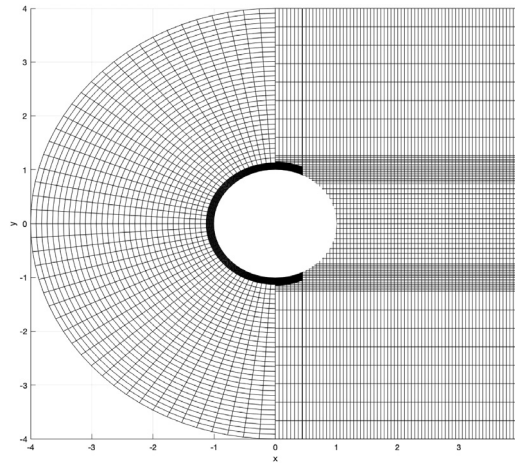


Fig. 6. A schematic image of the composite mesh  $\tilde{\Omega}_A^{N,M} \cup \hat{\Omega}_P^{N,M} \cup \Omega_S^{N,M}$ .

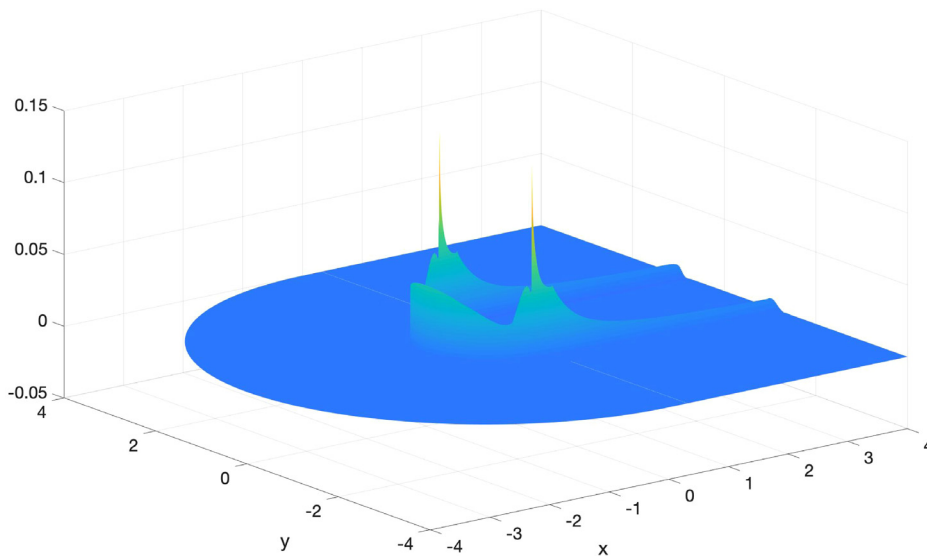


Fig. 7. Approximate global error  $\bar{U}_2^{128} - \bar{U}_2^{2048}$  in corrected approximation for  $\varepsilon = 2^{-10}$ .

ease of generating Tables, we have simply taken  $L = 2\sqrt{\min\{\delta, \varepsilon^{2/3} \ln 2048\}}$  in the patched region. When we include the patch, we observe convergence in Table 3 of the corrected approximations over this parabolic patch  $\Omega_P^N$  over an extensive range of  $\varepsilon$  and  $N$ . In Table 4, the global orders of convergence over the entire domain for the corrected approximation  $\bar{U}_2^N$  are given. These orders indicate that the corrected approximations are converging for all values of  $\varepsilon \in [2^{-20}, 1]$ . In the final Table 5, the approximate global errors over the entire domain are displayed for all  $\varepsilon \in [2^{-20}, 1]$ . We observe that as  $\varepsilon \rightarrow 0$  the global errors continue to grow for each fixed  $N$ . Hence, the method appears not to be parameter-uniform. Nevertheless, for any fixed value of  $\varepsilon$  we do observe convergence as  $N$  increases. In particular, we see in Figs. 7 and 8 that for the corrected approximations  $\bar{U}_2^N$ , the approximate global errors  $\bar{U}_2 - \bar{U}_2^{2048}$  essentially halve as the number of mesh points are doubled. This is in sharp contrast to the approximate global errors  $\bar{U}_1 - U_1^{2048}$  displayed in Figs. 4, 5.

The computed orders of convergence in Table 4 suggest that this multi-stage numerical method is producing a converging sequence of numerical approximations to the analytical solution of the Hemker problem (2) across the entire domain for singular perturbation values  $\varepsilon \in [2^{-20}, 1]$ .

### 6. Conclusions

Based on parameter explicit pointwise bounds on how the continuous solutions decays away from the circle, a numerical method was constructed for the Hemker problem. There are no spurious oscillations present in the numerical

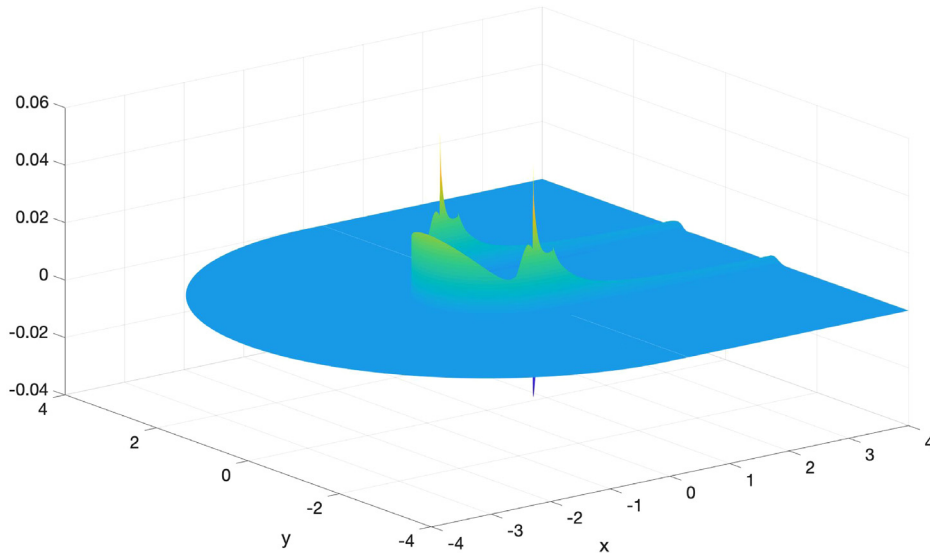


Fig. 8. Approximate global error  $\bar{U}_2^{256} - \bar{U}_2^{2048}$  in corrected approximation for  $\varepsilon = 2^{-10}$ .

Table 3

Computed double-mesh global orders of convergence  $\bar{p}_\varepsilon^N$  for the corrected approximations  $\bar{U}_C$  (17) measured over the patched region  $Q$  (13), where  $L = 2\sqrt{\min\{\delta, \varepsilon^{2/3} \ln 2048\}}$  and  $\delta = 0.05$ .

$\varepsilon N$	$N = 8$	16	32	64	128	256	512
1	1.4739	0.3521	0.6916	1.1128	0.7936	0.9664	0.9716
$2^{-2}$	1.7825	0.2514	0.4127	1.1106	0.6181	0.9426	0.9508
$2^{-4}$	1.4364	0.6690	0.4384	0.8073	0.6223	0.8619	0.4013
$2^{-6}$	0.2310	0.7570	1.5302	-0.6245	2.0571	0.5677	0.2180
$2^{-8}$	-0.2532	0.3617	0.8478	-0.0286	1.1685	1.2720	0.1293
$2^{-10}$	-0.0002	0.0086	0.4198	1.0663	1.6521	1.2344	0.8949
$2^{-12}$	-0.0208	-0.0051	0.1917	0.8547	1.4528	1.2501	1.0148
$2^{-14}$	0.1888	-0.0509	0.1504	0.5917	1.2201	1.3731	1.0606
$2^{-16}$	0.3670	-0.0685	0.0477	0.3999	1.0007	1.6196	1.1642
$2^{-18}$	0.3904	-0.0179	-0.0203	0.2101	0.7656	1.4258	1.3736
$2^{-20}$	0.7398	-0.2868	-0.0467	0.0795	0.5156	1.2055	1.6702
$\bar{p}_{R_\varepsilon}^N$	0.3593	0.0521	-0.0351	0.1095	0.5156	1.2055	1.6702

Table 4

Computed double-mesh orders of global convergence  $\bar{p}_\varepsilon^N$  for the corrected approximations  $\bar{U}_2$  (21) measured over the entire domain  $\Omega$ .

$\varepsilon N$	$N = 8$	16	32	64	128	256	512
1	2.0261	0.6227	0.2352	0.7464	0.8763	0.9448	0.9799
$2^{-2}$	2.0506	1.0501	0.3720	0.3373	0.8437	0.9907	0.4472
$2^{-4}$	1.9773	0.1282	1.9129	0.8324	0.3435	0.3734	-0.3310
$2^{-6}$	0.2310	0.7570	1.5302	-0.6245	2.5573	0.2520	0.0335
$2^{-8}$	-0.2532	0.3617	0.8478	-0.0286	1.1685	1.2720	0.1293
$2^{-10}$	-0.0002	0.0086	0.4198	1.0663	1.6521	1.2344	0.8949
$2^{-12}$	-0.0208	-0.0051	0.1917	0.8547	1.4528	1.2501	1.0148
$2^{-14}$	0.1888	-0.0509	0.1504	0.5917	1.2201	1.3731	1.0606
$2^{-16}$	0.3670	-0.0685	0.0477	0.3999	1.0007	1.6196	1.1642
$2^{-18}$	0.3904	-0.0179	-0.0203	0.2101	0.7656	1.4258	1.3736
$2^{-20}$	0.7398	-0.2868	-0.0467	0.0795	0.5156	1.2055	1.6702
$\bar{p}_{R_\varepsilon}^N$	0.3593	0.0521	-0.0351	0.1095	0.5156	1.2055	1.6702

solutions, as we use simple upwinding in all co-ordinate directions used. Several layer adapted Shishkin meshes are utilized and these grids are aligned both to the geometry of the domain and to the dominant direction of decay within the boundary/interior layer functions. Numerical experiments indicate that the method is producing accurate approximations

**Table 5**  
Approximate global errors  $\|\bar{U}_2^N - \bar{U}_2^{2048}\|_\Omega$  over the domain  $\Omega$ .

$\varepsilon N$	$N = 8$	16	32	64	128	256	512
1	0.1689	0.0828	0.0686	0.0435	0.0245	0.0127	0.0057
$2^{-2}$	0.2735	0.1434	0.0765	0.0530	0.0311	0.0197	0.0100
$2^{-4}$	0.4079	0.2272	0.1415	0.0887	0.0515	0.0305	0.0169
$2^{-6}$	0.5720	0.4206	0.2369	0.1186	0.1109	0.0330	0.0188
$2^{-8}$	0.6790	0.5657	0.4065	0.2034	0.1852	0.0650	0.0123
$2^{-10}$	0.7331	0.6325	0.4882	0.3030	0.1344	0.0518	0.0198
$2^{-12}$	0.7769	0.6916	0.5624	0.3859	0.1971	0.0698	0.0326
$2^{-14}$	0.8140	0.7414	0.6287	0.4662	0.2718	0.1100	0.0446
$2^{-16}$	0.8458	0.7847	0.6871	0.5419	0.3462	0.1615	0.0547
$2^{-18}$	0.8718	0.8213	0.7393	0.6122	0.4329	0.2280	0.0799
$2^{-20}$	0.8950	0.8519	0.7830	0.6720	0.5095	0.3025	0.1213

over an extensive range of the singular perturbation parameter. Hence, the method is stable for all values of the singular perturbation parameter and the numerical approximations are converging to the continuous solution for each value of the parameter; however, this convergence is not uniform in the singular perturbation parameter.

**Acknowledgment**

We wish to thank the anonymous reviewers for their meticulous reading of the paper and their insightful comments.

**Appendix. Bounds on the continuous solution**

1. For  $0 < \kappa \leq 1$ , consider the barrier function

$$B^-(x, y) := \begin{cases} e^{\frac{\kappa \cos(\theta)(r-1)}{\varepsilon}} & , \cos(\theta) \leq 0, \quad r \geq 1, \\ 1 & , x \geq 0, \quad x^2 + y^2 \geq 1 \end{cases} \tag{22}$$

For the subregion where  $x < 0$ , note the following expressions for the partial derivatives of this barrier function:

$$\begin{aligned} \tilde{B}_\theta^- &= -\frac{\kappa \sin(\theta)}{\varepsilon}(r-1)\tilde{B}^-; \\ \tilde{B}_{\theta\theta}^- &= -\left(\frac{\kappa \cos(\theta)}{\varepsilon}(r-1) - \frac{\kappa^2 \sin^2(\theta)}{\varepsilon^2}(r-1)^2\right)\tilde{B}^-; \\ \tilde{B}_r^- &= \frac{\kappa \cos(\theta)}{\varepsilon}\tilde{B}^-, \quad \tilde{B}_{rr}^- = \frac{\kappa^2 \cos^2(\theta)}{\varepsilon^2}\tilde{B}^-. \end{aligned}$$

Combining these expressions, we can deduce that

$$\begin{aligned} \tilde{L}\tilde{B}^- &\geq \frac{\kappa}{\varepsilon} \sin^2(\theta)\left(1 - \kappa + \frac{\kappa}{r}\right)\left(1 - \frac{1}{r}\right)\tilde{B}^- \geq 0, \quad \cos(\theta) \in (0, r)1; \\ \left[\frac{\partial B^-}{\partial n}\right]_{x=0} &= B^-_{,x}(0^-, y) = \frac{\kappa}{\varepsilon}\left(1 - \frac{1}{|y|}\right) \geq 0; \quad B^-(x, y) = 1, \quad x^2 + y^2 = 1; \quad \frac{\partial B^-}{\partial x}(R, y) = 0. \end{aligned}$$

Using Theorem 3 we establish the bound (3b).

2. Consider the following barrier function

$$B^+(x, y) := \begin{cases} e^{C_1(1+x)}e^{-\frac{(y-1)}{\sqrt{\varepsilon}}}, & y \geq 1; \quad C_1 \geq 2 \\ e^{C_1(1+x)}, & y \leq 1 \end{cases}$$

In the region where  $y > 1$ , note the following expressions for the partial derivatives of this function:

$$B^+_x = C_1 B^+ \quad \text{and} \quad -\varepsilon B^+_{yy} = -B^+$$

and so, for  $\varepsilon$  sufficiently small,

$$L B^+ = (C_1 - \varepsilon C_1^2 - 1)B^+ \geq 0, \quad \forall y > 1.$$

Note also that

$$B^+(x, y) \geq 1, \quad \text{if} \quad x^2 + y^2 = 1; \quad \left[\frac{\partial B^+}{\partial n}\right]_{y=1} = -B^+_y(x, 1^+) > 0 \quad \text{and} \quad B^+_x(R, y) \geq 0.$$

Using Theorem 3 we establish the bound (3c) for  $y > 0$  and using symmetry we deal with the case of  $y < 0$ .

3. For  $y > 0$ , consider the following function, defined in a neighborhood of the line  $x = 0$ ,

$$B(x, y) := \left(1 + \frac{\alpha x}{\varepsilon^{1/3}}\right)(1 - \alpha C)^{-1} e^{-\frac{\kappa(0.5x^2 + y - 1)}{\varepsilon^{2/3}}}, \quad -C\varepsilon^{1/3} < x < C\varepsilon^{1/3}, \quad \alpha C < 1;$$

where the possible ranges for the positive parameters  $\alpha, \kappa, C$  will be specified below. Note the following expressions for the partial derivatives of this function:

$$\begin{aligned} B_x &= \frac{(1 - \alpha C)^{-1}}{\varepsilon^{1/3}} \left(\alpha - \frac{\kappa x}{\varepsilon^{1/3}} \left(1 + \frac{\alpha x}{\varepsilon^{1/3}}\right)\right) e^{-\frac{\kappa(0.5x^2 + y - 1)}{\varepsilon^{2/3}}}; \\ \varepsilon B_{yy} &= \frac{\kappa^2(1 - \alpha C)^{-1}}{\varepsilon^{1/3}} \left(1 + \frac{\alpha x}{\varepsilon^{1/3}}\right) e^{-\frac{\kappa(0.5x^2 + y - 1)}{\varepsilon^{2/3}}}; \\ \tilde{B}_{xx} &= \frac{1}{\varepsilon} O(\varepsilon^{1/3}) e^{-\frac{\kappa(0.5x^2 + y - 1)}{\varepsilon^{2/3}}}, \quad -C\varepsilon^{1/3} < x < C\varepsilon^{1/3}. \end{aligned}$$

Let us introduce  $\xi := x\varepsilon^{-1/3}$ , then for  $\xi \in C(-1, 1), 0 < \alpha C < 1$ ,

$$\begin{aligned} -\varepsilon B_{yy} + B_x &= \frac{(1 - \alpha C)^{-1}}{\varepsilon^{1/3}} (\alpha - \kappa\xi(1 + \alpha\xi) - \kappa^2(1 + \alpha\xi)) e^{-\frac{\kappa(0.5x^2 + y - 1)}{\varepsilon^{2/3}}} \\ &\geq \frac{1}{\varepsilon^{1/3}} \left(\frac{\alpha}{(1 + \alpha C)} - C\kappa - \kappa^2\right) e^{-\frac{\kappa(0.5x^2 + y - 1)}{\varepsilon^{2/3}}}. \end{aligned}$$

In order that  $LB(x, y) \geq 0, x \in C\varepsilon^{1/3}(-1, 1)$  (and recalling that  $\alpha C < 1$ ) we impose the following constraints:

$$\kappa \leq \frac{C}{3}, \quad \alpha > \frac{8}{9}C^2, \quad C^3 < \frac{9}{8}. \tag{23}$$

For simplicity, we take the particular values,

$$C = 1, \quad \alpha = 0.9 \quad \text{and} \quad \kappa = \frac{1}{3}.$$

From this,

$$B_x(x, y) > 0, \quad B_y(x, y) < 0; \quad -\varepsilon^{1/3} \leq x \leq \varepsilon^{1/3}, \quad y > 0.$$

By restricting the domain of the function  $B(x, y)$  to the strip

$$S := \{(x, y) \mid |x| < \varepsilon^{1/3}, -\mu\varepsilon^{2/3} < 0.5x^2 + y - 1 < \mu\varepsilon^{2/3}\}$$

then  $e^{\kappa\mu} \geq B(x, y) \geq e^{-\kappa\mu}, (x, y) \in \bar{S}$  and

$$e^{\kappa\mu} B(x, y) \geq 1 \geq u(x, y), \quad (x, y) \in \bar{S} \setminus S.$$

Using [Theorem 1](#) we establish the bound (3d) for  $y > 0$  and using symmetry we deal with the case of  $y < 0$ .

**References**

[1] P.W. Hemker, A singularly perturbed model problem for numerical computation, *J. Comp. Appl. Math.* 76 (1996) 277–285.  
 [2] M. Augustin, A. Caiazzo, A. Fiebach, J. Fuhrmann, V. John, A. Linke, R. Umla, An assessment of discretizations for convection-dominated convection-diffusion equation, *Comput. Methods Appl. Mech. Engrg.* 200 (47–48) (2011) 3395–3409.  
 [3] B. García-Archilla, Shishkin mesh simulation: a new stabilization technique for convection–diffusion problems, *Comput. Methods Appl. Mech. Engrg.* 256 (2013) 1–16.  
 [4] E.D. Havik, P.W. Hemker, W. Hoffmann, Application of the over-set grid technique to a model singular perturbation problem, *Computing* 65 (4) (2000) 339–356.  
 [5] V. John, L. Schumacher, A study of isogeometric analysis for scalar convection–diffusion equations, *Appl. Math. Lett.* 27 (2014) 43–48.  
 [6] P.A. Lagerstrom, *Matched Asymptotic Expansions: Ideas and Techniques*, Applied Mathematical Sciences, Vol. 76, Springer-Verlag, New York, 1988.  
 [7] G. Barrenea, V. John, P. Knobloch, R. Rankin, A unified analysis of algebraic flux correction schemes for convection–diffusion equations, *SeMA J. Bol. Soc. Espan. Mat. Apl.* 75 (4) (2018) 655–685.  
 [8] H. Han, Z. Huang, R.B. Kellogg, A tailored finite point method for a singular perturbation problem on an unbounded domain, *J. Sci. Comput.* 36 (2) (2008) 243–261.  
 [9] W. Eckhaus, Boundary layers in linear elliptic singular perturbation problems, *SIAM Rev.* 14 (1972) 225–270.  
 [10] A.M. Il’in, Matching of Asymptotic Expansions of Solutions of Boundary Value Problems, in: *Mathematical Monographs*, vol. 102, American Mathematical Society, 1992.  
 [11] R.T. Waechter, Steady longitudinal motion of an insulating cylinder in a conducting fluid, *Proc. Camb. Philos. Soc.* 64 (1968) 1165–1201.  
 [12] G.I. Shishkin, *Discrete Approximation of Singularly Perturbed Elliptic and Parabolic Equations*, Russian Academy of Sciences, Ural section, Ekaterinburg, 1992, (in Russian).  
 [13] P.A. Farrell, A.F. Hegarty, J.J.H. Miller, E. O’Riordan, G.I. Shishkin, *Robust Computational Techniques for Boundary Layers*, Chapman and Hall/CRC Press, Boca Raton, 2000.  
 [14] A.F. Hegarty, E. O’Riordan, in: G. R. Barrenea Glasgow, J. Mackenzie (Eds.), *A Numerical Method for the Hemker Problem*, Boundary and Interior Layers - Computational and Asymptotic Methods, BAIL 2018, in: *Lecture Notes in Computational Science and Engineering*, vol. 135, Springer, 2020, pp. 97–111.

- [15] J.J.H. Miller, E. O'Riordan, G.I. Shishkin, *Fitted Numerical Methods for Singular Perturbation Problems*, World-Scientific, 2012, Revised edition.
- [16] E. O'Riordan, G.I. Shishkin, A technique to prove parameter-uniform convergence for a singularly perturbed convection-diffusion equation, *J. Comp. Appl. Math.* 206 (2007) 136–145.
- [17] E. O'Riordan, G.I. Shishkin, Parameter uniform numerical methods for singularly perturbed elliptic problems with parabolic boundary layers, *Appl. Numer. Math.* 58 (2008) 1761–1772.
- [18] M.H. Protter, H.F. Weinberger, *Maximum Principles in Differential Equations*, Springer-Verlag, New York, 1984.
- [19] A.F. Hegarty, E. O'Riordan, A parameter-uniform numerical method for a singularly perturbed convection-diffusion problem posed on an annulus, *Comput. Math. Appl.* 78 (10) (2019) 3329–3344.
- [20] R.K. Dunne, E.O. Riordan, G.I. Shishkin, Fitted mesh numerical methods for singularly perturbed elliptic problems with mixed derivatives, *IMA J. Numer. Anal.* 29 (2009) 712–730.